Eur. Phys. J. A **30**, 275–291 (2006)
DOI 10.1140/epja/i2006-10123-8

THE EUROPEAN PHYSICAL JOURNAL A

Detection

R.T. de Souza[1], N. Le Neindre[2,a], A. Pagano[3], and K.-H. Schmidt[4]

[1] Indiana University Cyclotron Facility, Indiana University, Bloomington, IN 47405, USA
[2] Institut de Physique Nucléaire d'Orsay, CNRS-IN2P3, F-91406 Orsay, France
[3] Istituto Nazionale di Fisica Nucleare INFN and Università di Catania, I-95123 Catania, Italy
[4] GSI mbH, D-64291 Darmstadt, Germany

Received: 4 April 2006 /
Published online: 24 October 2006 –

Abstract. This review on second- and third-generation multidetectors devoted to heavy-ion collisions aims to cover the last twenty years. The presented list of devices is not exhaustive but regroups most of the techniques used during this period for nuclear reactions at intermediate energy ($\simeq 10\,A$ MeV to $1\,A$ GeV), both for charged-particle and neutron detection. The main part will be devoted to 4π multidetectors, projectile decay fragmentation, high-resolution magnetic spectrometers, auxiliary detectors and neutron detection. The last part will present the progress in electronics and detection in view of the construction of future-generation detectors.

PACS. 29.30.Aj Charged-particle spectrometers: electric and magnetic – 29.40.Cs Gas-filled counters: ionization chambers, proportional, and avalanche counters – 29.40.Mc Scintillation detectors – 29.40.Wk Solid-state detectors

1 Introduction

The empirical knowledge of the dynamics and the thermodynamics with nuclear degrees of freedom emerges from experimental studies of nuclear collisions. For this purpose, powerful experimental installations have been developed at many accelerator facilities with the aim of registering as many observables of the reaction products as possible with the best possible resolution. The key properties of these installations are large solid-angle coverage, high granularity and low detection thresholds. Generally, one strives for observation and full identification of all reaction products. For charged particles, the determination of the atomic number Z has become standard, while isotopic identification is still limited to the lighter products in most installations.

Full isotopic identification of all residues has become an important issue, and strong efforts are being made to achieve this goal. The attempts follow two roads: On the one hand, detector telescopes are being developed with ToF or pulse-shape analysis to extend the mass range where isotopic resolution can be achieved. On the other hand, full identification over the whole mass range has been obtained by using powerful magnetic spectrometers.

Motivated by specific characteristics of the reaction dynamics, experiments are performed from the Fermi-energy regime up to the GeV-per-nucleon range, in accordance with the capabilities of the corresponding accelerators. Traditionally, most experiments have been performed in the Fermi-energy regime, where the partly overlapping Fermi spheres of projectile and target lead to very specific features like isospin diffusion. Reactions at energies around $1\,A$ GeV, where the Fermi spheres of projectile and target are well separated, are rather goverened by a clear distinction of participant and spectator nucleons.

Different requirements are imposed on the detector equipment for these different energy regimes. Experiments at low energies need large angular coverage. Higher energies lead to a strong kinematical focussing of projectile-like reaction products in the forward direction. They also facilitate full identification of heavy residues in mass and atomic number and high-precision measurements of their kinematic properties as well as the simultaneous detection of neutrons and charged particles.

2 Heavy ions

This section presents the most important 4π multidetectors, *i.e.* devices covering as much of the solid angle as possible, used during the last twenty years all over the world. With the evidencing of multifragmentation in the early 1980s, multidetectors able to detect most of the products coming from reactions between heavy-ion collisions became essential. Following the progress made in microelectronics, detection and in understanding the new phe-

[a] e-mail: leneindre@ipno.in2p3.fr

nomena, always more and more powerful devices appeared with always better and better granularity, better angular coverage, lower detection thresholds, and better identification (including isotopic resolution).

2.1 NAUTILUS

The NAUTILUS multidetector installed at Ganil was constituted by four multidetectors, DELF, XYZt, MUR and TONNEAU [1].

2.1.1 General characteristics

- DELF and XYZt:
  - position-sensitive gas telescope consisting of a parallel-plate avalanche detector and an ionization chamber;
  - full fragment efficiency for $Z \geq 8$;
  - angular coverage 3°–150°;
  - DELF: detection thresholds 0.13 A MeV, angular resolution $\Delta\theta = 0.5°$, velocity resolution $\Delta v/v = 4\%$;
  - XYZt: detection thresholds 2.0 A MeV, angular resolution $\Delta\theta = 0.1°$, velocity resolution $\Delta v/v = 7\%$.
- MUR and TONNEAU:
  - plastic scintillators for light-charged-particle detection $Z = 1$–2;
  - energy thresholds 1 A MeV;
  - angular coverage 3°–150°.
- Complete device: 35% of 4π.

Fragments and particles produced in the heavy-ion collisions were detected by the four multidetectors of NAUTILUS. DELF and XYZt are gaseous multidetectors in which each module was constituted by a parallel-plate avalanche detector for localisation and an ionization chamber. They detected with full efficiency fragments of charge greater than eight and their angular coverage was between 3° and 150°, which corresponds to almost 2π. For DELF, energy detection thresholds were 0.13 A MeV, the angular resolution $\Delta\theta = 0.5°$ and the velocity precision $\Delta v/v = 4\%$. For XYZt, energy detection thresholds were 2 A MeV, the angular resolution $\Delta\theta = 0.1°$ and the velocity precision $\Delta v/v = 7\%$. The MUR and TONNEAU were constituted by scintillation plastics which detected light charged particles (essentially $Z = 1$–2), with an energy threshold of about 1 A MeV. They covered an angular range between 3° and 150° representing 70% of 4π.

When XYZt and DELF were mounted inside the reaction chamber they shadowed the MUR and TONNEAU multidetectors reducing thus their detection efficiency for light charged particles to 35% of 4π. Before being detected, particles lose energy in the fragment detectors. Therefore, detection thresholds were higher, of the order of 4 A MeV, and there was degradation in the quality of time-of-flight measurements (light-particle velocities). This was mainly the case for particles emitted by the quasi target. Nevertheless, in spite of these drawbacks on light charged particles, this device was perfectly adapted for fission studies. The very low-energy thresholds allowed the detection of fragments emitted by the target side both for residues and fission fragments and projectile fragments which benefited from the recoil energy of the emitting nucleus to largely overcome the thresholds.

2.2 MSU 4π

Michigan State University 4π multidetector.

2.2.1 General characteristics

- Soccer ball geometry.
- $18° \leq \theta \leq 162°$.
- 215 fast (3 mm) - slow plastic (25 cm).
- 55 Bragg curve detectors.
- Thresholds:
  - 17 A MeV for plastic only;
  - few A MeV with Bragg curve detectors.
- p, d, t, He, Li, Be, B, C with $E/A \leq 200$ MeV.

2.2.2 Main results

Thanks to the measurements of the momentum in an event, the MSU 4π device allowed the determination of the "balance energy" at which the nuclear potential changes from attractive to repulsive. The momentum dependence of the mean field is one of the basic ingredients of transport models of any kind. The analysis performed with such a multidetector has permitted to extract the evolution of the balance energy with beam energy as a function of the reduced impact parameter, bringing thus important constraints for the models.

2.3 MSU MINIBALL

Michigan State University MINIBALL [2].

2.3.1 General characteristics

- 188 detectors: $9° \leq \theta \leq 160°$.
- Large angular coverage 89% of 4π.
- Thin fast plastic (40 μm) - CsI(Tl) (2 cm).
- Thresholds: 1.5 A MeV for ^{4}He up to $\simeq$ 3 A MeV around Ca.
- Charge identification for $Z \leq 18$ and mass separation for $Z = 1$–2.

2.3.2 Main results

The fragment detection with low thresholds and good coverage allowed the investigation of the dependence of fragment number on total charge multiplicity (dissipation) and incident beam energy [3]. Thanks to the reasonable energy and angular resolution, IMF-IMF correlations were performed giving information on the mean time between IMF emissions. Times as short as 100–200 fm/c were found depending on the relative momentum between the two partners [3].

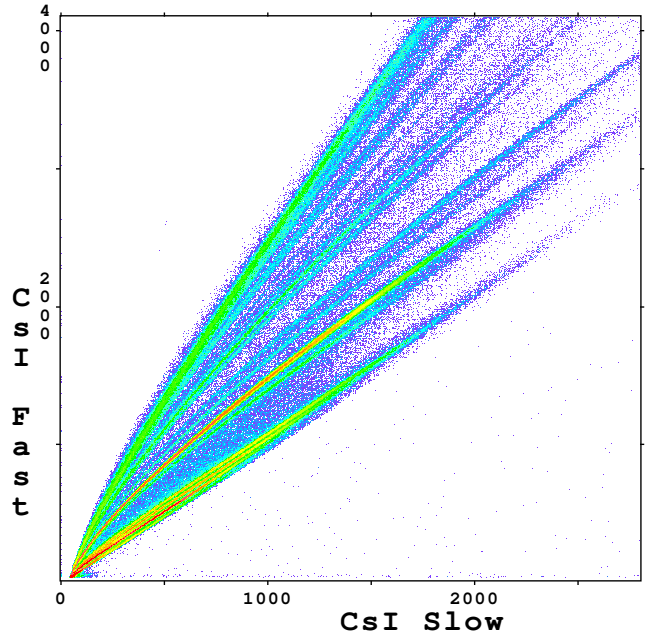

Fig. 1. Fast-slow INDRA CsI matrix obtained by accumulating high-energy light charged particles coming from two reactions, ^{124}Xe + ^{112}Sn and ^{136}Xe + ^{124}Sn at 45 A MeV, during the fifth INDRA campaign at Ganil. Isotopic identification is obtained for H, He, Li, Be and B produced during the collisions.

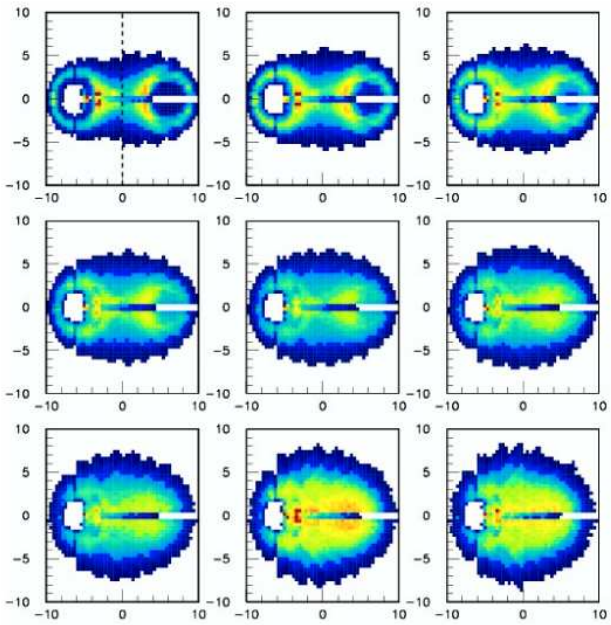

Fig. 2. Alpha-particle centre-of-mass $v_{parallel}$-$v_{perpendicular}$ plots for different dissipation regimes measured with the INDRA multidetector in Xe + Sn collisions at 80 A MeV. Peripheral to central collisions are displayed from upper-left to bottom-right panel (M. Pichon, PhD Thesis, Caen University (2004)).

2.4 INDRA

Identification de Noyaux et Détection avec Résolution Accrues [4].

2.4.1 Main characteristics

- Large angular coverage: 90% of 4π.
- High granularity provided by 336 telescopes distributed on 17 rings from 2° to 176°.
- Phoswich or Si-CsI telescopes: 2° to 3°.
- Ionization chamber-Si-CsI telescopes: 3° to 45°.
- Ionization chamber-CsI telescopes: 45° to 176°.
- Low-energy thresholds, around 0.8 A MeV for $Z \leq 12$ and $\simeq 1.3\,A$ MeV above.
- Charge identification for all Z.
- Mass identification for $1 \leq Z \leq 4$, see fig. 1 (to be extended to $Z \simeq 10$ with optimum electronic gain and software, in progress).

2.4.2 Main advantages

INDRA is one of the first 4π multidetectors of the second generation dedicated to multifragmentation studies. The large solid angular coverage of INDRA, 90% of 4π, can be seen in fig. 2. Alpha-particle centre-of-mass $v_{parallel}$-$v_{perpendicular}$ plots are shown for different dissipation regimes. Starting from peripheral collisions (upper-left panel), we clearly see Coulomb rings caracterisctic of an evaporation regime. At the opposite, for more central collisions (bottom-right panel), a quasi-homogeneous emission is seen in the centre of mass.

Over more than ten years, INDRA has proved its reliability during four campaigns of measurements at Ganil-France, plus a campaign conducted at GSI-Germany. It has also proved its versatility, as it was coupled with the first CHIMERA ring in 1997, it was associated to other telescopes for time-of-flight measurements, position-sensitive telescopes for crystal-blocking experiments on fission lifetimes of super-heavy elements, and it is scheduled to be moved and coupled to the Vamos spectrometer at Ganil for residue identification of compound nuclei. Symmetric as well as asymmetric systems, in both reverse and direct kinematics, for projectile energies as small as $\simeq 5\,A$ MeV and as large as 1 A GeV (for C beams at GSI) have been recorded since 1993. We have learnt, during all these experiments, that if INDRA is well suited for studying central collisions of symmetric systems, nevertheless this detector has some drawbacks concerning asymmetric systems where the centre-of-mass velocity is small (Ni + Au 32 A MeV, C + Sn). In these cases the lack of time-of-flight measurements (*i.e.* very low-energy thresholds) for very slow fragments leads to a reduced detection quality (especially at backward angles).

2.4.3 Main INDRA results

INDRA is able to perform physics analyses as different as the study of vaporization of a quasi projectile (Ar + Ni),

studies of fission products (U + U, Ta + Au, Au + Au), central collisions leading to fusion-like sources (Xe + Sn, Ni + Au, Ni + Ni), de-excitation studies on a large scale of dissipation for hot nuclei (mainly quasi projectile), evidence of mid-rapidity emission, neck, ... Because of its good detection properties, intra-event correlations were studied leading to various results in many domains: impact parameter estimation, determination of the reaction plane for spin measurements, calorimetry event by event, reconstruction of hot primary fragments. With such an efficient tool all main subjects of heavy-ion collisions at intermediate energies were covered:

- Phase transition: with temperature measurements (caloric curve), studies of negative heat capacities, abnormal fluctuations (Delta scaling), scaling laws (Fisher's scaling, critical exponents, ...), bimodality of an order parameter, spinodal decomposition, phase diagram, random break-up, etc.
- Reaction mechanism: mid-rapidity emission, neck formation, fusion-like events, fission, momentum transfer, frag-ment-formation mechanism, isospin equilibration, chrono-meter of the fragmentation process, ...
- De-excitation of hot nuclei: from evaporation to vaporization, passing through fission, multifragmentation of any kind, ...
- Comparison with models: statistical models (MMMC, SMM, MMM, Simon, Gemini), dynamical models (QMD, AQMD, CNBD, HIPSE, BNV, BUU, stochastic mean-field approach (BOB)), lattice gas, EES, etc.

2.4.4 To go forward

With the increasing availability in the near future of radioactive nuclear beams (Spiral, Spiral II, Eurisol), the role of the isospin degree of freedom in nuclear reactions will be studied. Such a study will require a new generation of 4π multidetectors keeping all the qualities of the present generation (low-energy thresholds, granularity) and representing a step forward in terms of isotopic identification (both charge and mass for nuclei up to $Z \simeq 30$), always a better granularity for more precise intra-event correlation functions and also a coupling with neutron detectors (see recommendations from NuPECC long-range plan 2004). A French-Italian group has been working on this subject during the last four years. Its main goal is an R&D program on the feasibility of such a new detector. The name of this project is FAZIA (Four π A-Z Identification Array). For this goal, NTD silicon detectors, CsI scintillators and associated digital electronics are being tested. A report on the feasibility of such a new project is in progress.

2.5 CHIMERA

Charged Heavy Ion Mass and Energy Resolving Array [5].

2.5.1 General characteristics

- 9×2 rings in the range $1^\circ \leq \theta \leq 30^\circ$.
- The sphere: 17 rings in the range $30^\circ \leq \theta \leq 176^\circ$.
- For an amount of 1192 Si-Csi(Tl) telescopes with time-of-flight measurements.
- Very high granularity and efficiency: 94% of 4π.
- Mass identification at very low energy $< 0.3\,A$ MeV for heavy ion (TOF).
- Z and A identification by ΔE-E for $Z \leq 9$.
- Z and A identification for high-energy light charged particles (using fast-slow components on CsI(Tl) signals) $Z \geq 5$.
- Z identification up to beam charge for $Z > 9$ (ΔE-E).

2.5.2 Physics goals

CHIMERA is the last example of second-generation 4π detector. The high granularity of the detector, its high solid angular coverage, its low-energy thresholds allow to work in different experimental conditions, reverse or direct kinematics, symmetric or asymmetric systems, small or heavy nuclei (target-projectile).

Thanks to its good capabilities, many aspects of physics in heavy-ions collisions can be studied [6]: starting from dynamical aspects (fragment formation from projectile, target or neck emission, time scale in neck fragmentation, mid-velocity emission, pre-equilibrium effects, isospin equilibration in time, ...), thermodynamical characteristics (exploration of the phase diagram in temperature, excitation energy, density, volume, isospin, signals of phase transition in hot nuclear matter, isoscaling in multifragmenting sources, ...) as well as prospective experiments (Bose condensates, search for alpha-particle condensates in hot diluted nuclei).

2.5.3 CHIMERA-PS —upgrading

In the near future (2006) an upgrade of the CHIMERA electronics will appear. The new method consists in the rise time measurement for pulse-height application. It results in a charge identification up to $Z \simeq 10$ with a $\simeq 4\,A$ MeV energy threshold for particles stopped in silicon detectors, see fig. 3. It will be coupled with time-of-flight identification that gives both A and Z for low-energy light fragments.

2.6 GARFIELD

General ARray for Fragment Identification and for Emitted Light particles in Dissipative collisions [7].

2.6.1 General characteristics

- High granularity (400 ΔE-E telescopes $\theta \simeq 4^\circ$–150°).
- Low-energy thresholds (ionization chambers as ΔE).
- A and Z identification ($1 \leq Z \leq 8$) up to $\theta \simeq 90^\circ$.
- Digital electronics for pulse-shape discrimination.

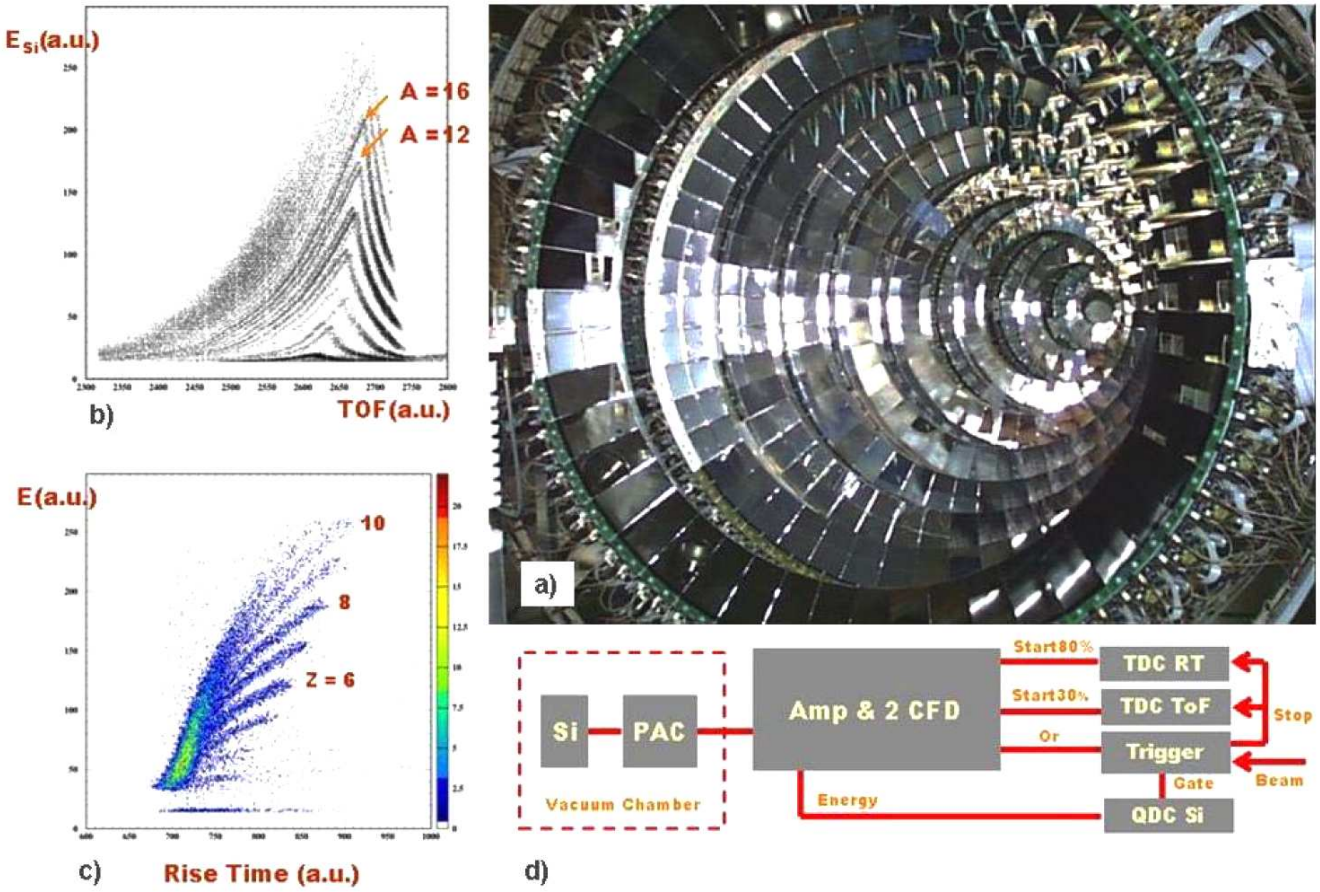

Fig. 3. a) Forward part of the CHIMERA detector (as seen by the target). b) Energy plot from silicon detector *vs.* time of flight for reaction products of Ne + Al at 20 A MeV (detected at $\theta = 12^\circ$ and at 180 cm from the target). Charged particles stopped (low kinetic energy) in the first stage silicon detector or (alternatively) stopped in the second stage CsI(Tl) crystal are seen in the plot. c) Energy plot *vs.* signal rise time showing the charge identification obtained with the PSD only for charged particles that are stopped in the silicon detector. d) Upgraded electronics chain of CHIMERA for the PSD analysis with silicon detectors.

2.6.2 The GARFIELD drift chamber

- 180 double-stage E (CsI(Tl))-ΔE (Multi segmented gas chamber) telescopes.
- Angular coverage: (30°–85°, 95°–150°).
- Charge resolution from proton to heavy ions, with $\Delta Z/Z = 1/28$.
- Angular resolution ($\Delta\theta = 1^\circ$, $\Delta\phi = 7.5^\circ$).

2.6.3 Scientific goals

Installed at the LNL Legnaro Italy, GARFIELD is used by the Nucl-ex Collaboration whose main interest is the study of the dynamics and thermodynamics of reactions at low-to-medium energy. It is designed to detect and identify with low-energy thresholds both light charged particles and heavy fragments. It is based on a gas drift chamber which conveys primary ionization electrons on gas microstrip devices where multiplication occurs and the energy-loss signals are generated. Silicon detectors or CsI(Tl) crystals operate as residual-energy detectors. This detector can be coupled to other systems like the MULTICS phoswich scintillators [8] or Hector (8 large BaF_2 detectors) according to the physic (mechanism) one wants to study.

2.7 FIASCO

Florentine Initiative After Superconducting Cyclotron Opening [9].

2.7.1 General characteristics

- 24 positive position-sensitive gas detectors, Parallel-Plate Avalanche Detectors (PPADs), for velocity-vector determination of heavy fragments $A > 20$.
- 96 silicon telescopes for the measurements of projectile-like fragment products (energy and charge).

– 158 phoswich modules for light charged particles and small fragments $3 \leq Z \leq 20$.
– Time-of-flight measurements.

2.7.2 Main goals and topics

The FIASCO multidetector is a low-threshold apparatus, optimized for the investigation of peripheral to semi-central collisions in heavy-ion reactions at Fermi energies. It consists of three types of detectors. The first detector layer is a shell of 24 position-sensitive Parallel-Plate Avalanche Detectors PPADs, covering about 70% of the forward hemisphere, which measure the velocity-vectors of heavy ($Z \geq 10$) reaction products. Below and around the grazing angle, behind the most forward PPADs, there are 96 ΔE-E silicon telescopes (with thickness of 200 and 500 μm, respectively); they are mainly used to measure the energy of the projectile-like fragment and to identify its charge and, via the time of flight of the PPADs, also its mass. Finally, behind most of the PPADs there are 158 (or 182, depending on the configuration) scintillation detectors, mostly of the phoswich type, which cover 25–30% of the forward hemisphere; they identify both light charged particles ($Z = 1$–2) and intermediate-mass fragments ($3 \leq Z \leq 20$) measuring also their time of flight. It was specifically designed and built by the Heavy-Ion Group of the INFN and the Department of Physics of the University of Florence for studying non-central collisions in heavy-ion reactions at Fermi energies (15–40 A MeV) with the beam delivered by the superconducting cyclotron of the Laboratori Nazionali del Sud, LNS in Catania, Italy.

2.8 NIMROD

Neutron Ion Multidetector for Reaction Oriented Dynamics [10].

2.8.1 General characteristics

The charged-particle detector setup is composed of:

– 176 CsI(Tl) arranged in 13 rings:
- 6 rings of 12 detectors in the range 3.5°–27.8°;
- 2 rings of 24 detectors in the range 28.7°–45°;
- 2 rings of 16 detectors in the range 48.3°–75°;
- 1 rings of 8 detectors in the range 75°–105°;
- 1 rings of 8 detectors in the range 105°–135°;
- 1 rings of 8 detectors in the range 135°–170°.
– For the four forward rings, 20 silicon telescopes composed for each ring by
- 2 × (150 + 500 microns) (Super Telescopes) isotopic resolution for $Z \leq 8$;
- 1×150 microns (Z identification for all particles ΔE-E technique);
- 2×300 microns (Z identification for all particles ΔE-E technique)
placed in front of 5 CsI scintillators in each ring.
– 96 ionization chambers.

NIMROD is a 4π neutron and charged-particle detection system built at Texas A&M to study reaction mechanisms in heavy-ion reactions. It is used to select collisions according to their violence. Dynamic and thermodynamic information is derived from the observed multiplicities, energies and angular distributions of particles and fragments produced in the nuclear reaction. Neutrons are detected using a liquid scintillator which is contained in vessels around the target. The charged-particle detectors are composed of ionization chambers, silicon telescopes and CsI(Tl) scintillators covering angles between 3 and 170 degrees. These charged-particle detectors are placed in a cavity inside the revamped TAMU (Texas A&M University) neutron ball. To minimize the cost of the detector, the "INDRA geometry" was adopted in the forward direction. The forward rings of detectors thus cover polar angles from 3.6 to 45 degrees in 8 concentric rings of 12 CsI(Tl) detectors each. This arrangement completes the already existing TAMU CsI Ball array which is used almost "as is" from 45–170 degrees.

2.9 FOPI

FOur PI (π) detector for charged particles [11].

2.9.1 General characteristics

– Superconducting solenoid.
– Forward plastic wall.
– Forward drift chamber.
– Central drift chamber.
– Plastic barrel.

The FOPI detector has documented the investigation of the fragments and the particles produced in central heavy-ion collisions. This detector detects, identifies, and determines the momentum of all charged particles emitted in a heavy-ion reaction. Based on the modular combination of different detector systems, the total assembly achieves its goal of covering the complete range of beam energies (0.1–2 GeV per nucleon) made available by GSI's SIS heavy-ion synchrotron. The target is located within a superconducting coil, which produces a magnetic field of 0.6 tesla. Charged particles within this field travel along curved paths before passing through the drift chambers. These chambers register both the particle track and the energy loss suffered by the particle in its passage through the detector gas. In addition, lines have been drawn through connected hits, which have been recognized by the automatic track-recognition of the event. Further on through the detector, the majority of the particles land in scintillation counters, with which their flight time from the target can be determined. The combination of different measurements enables the unambiguous identification of the particles.

The FOPI detector's potential ability to identify particles is, however, not restricted to charged particles. Although neutral particles do not themselves leave signals in

the detector system, some of them can be recognized and reconstructed thanks to their decay. This interesting class of particles includes neutral particles containing a strange quark, such as the neutral kaon and the Λ-particle. Due to their strangeness, they are relatively long-lived, decaying after a flight of several centimeters into charged particles, which leave tracks in the detectors. As the momenta and particle types are already known, the calculation of the invariant masses and comparison with the rest masses of the candidate particles enable the direct determination of which tracks belong together.

2.9.2 Main results

The FOPI detector can simultaneously detect all the charged and some of the neutral particles produced in a heavy-ion reaction. Global correlations among the particles are thus possible. Also known as collective effects, these correlations provide meaningful signatures for the properties of nuclear matter. Main results concern: collective expansion, stopping and directed sidewards flow at the highest energies, the latter of which provides interesting information, particularly in the case of strange particles, on interactions with the surrounding matter (in-medium effect) [12].

Collective expansion
An interpretation of the FOPI results leads to the conclusion that the observed fragments arise from an expanding flow of matter, from which they all carry the same velocity component into the detector. Although the density is not directly accessible from the measurements, comparison of the spectra and the rapidity-density distribution has been used with the predictions of so-called transport models to determine the change in the density over time and the maximum density reached. For heavy systems, a beam energy of 1 GeV per nucleon produces approximately the double density of the ground state. Variation of the beam energy and of the projectile-target combination enables the region between one and 2.5 times normal density to be covered.

Directed sidewards flow
The question of how generated particles, in particular vector mesons and kaons, behave under conditions of high temperature and density was investigated. It would appear that the observed probabilities of production of the antikaons in particular can currently only be described theoretically if it is assumed that particle masses are lower in-medium. Another window on possible "in-medium properties" of kaons is founded upon the directed sidewards flow. As nuclear matter is extremely difficult to compress, the particles attempt to get out of the way. Theoretically one expects a change of hadron properties in hot and dense nuclear matter. Thus, strange particles are ideal probes for in-medium effects. FOPI capabilities in this detection domain have brought strong information in this field.

Stopping
Rise and fall of the stopping properties in nuclear matter was investigated both with incident energy and its size dependence. It was found that stopping is maximal around $\simeq$ 400 A MeV and decreases toward higher beam energies. Stopping increases also with system size (Au + Au as compared to Ca + Ca), and systems exhibit always transparency, which increases with higher beam energy. It was also shown that stopping in nuclear matter is correlated with flow and pressure measurements.

2.10 MEDEA

Multi Element DEtector Array for γ-rays and light-charged-particles detection [13].

2.10.1 General characteristics

- 180 BaF2 scintillator crystal detectors.
- 120 plastic phoswich detectors.
- Spherical geometry around the target.
- Angular coverage: 90% of 4π.
- Gamma-ray detection up to $\simeq$ 300 MeV.
- + Light-charged-particle detection.

MEDEA's basic configuration consists of 180 barium fluoride scintillator crystals, arranged in the shape of a ball, plus a forward-angle wall of 120 phoswich detectors. The inner radius of the ball (22 cm) and the distance of the wall from the target (55 cm) allow the placement of other detectors in the inner volume. MEDEA was first installed at Ganil (France) in 1989-1993 and then moved to the Laboratori Nazionali del Sud in Catania (Italy). Coupled with other detectors like Multics [8], MEDEA has given its contribution to intermediate-energy physics, both in the field of fragment production and in pre-equilibrium production of particles and γ-rays. The hot giant dipole resonance GDR has been also investigated taking advantage of the coupling with the superconducting solenoid SOLE and its focal-plane detector MACISTE (Mass And Charge Identification Spectroscopy with TElescope (gas chamber for ΔE-wire chamber for x-y position and TOF-plastic scintillator for E)) [13] installed at the LNS-Catania.

3 Auxiliary detectors

3.1 LASSA

Large-Area Silicon-Strip Array.

3.1.1 General characteristics

- Highly segmented Si(65 μm)-Si(0.5–1.5 mm)-Csi(Tl) 4–6 cm read out by photodiode.
- Each silicon segmented in 16–32 strips covered by 4 CsI.
- 10% thickness variation in ΔE.

– Segmentation helps both particle identification and angular resolution.
– Angular resolution $\Delta\theta \simeq 0.8°$.
– 9 to 20 telescopes.
– Thresholds: 2 A MeV for ^{4}He, 4 A MeV for ^{12}C.
– Isotopic identification for $Z \leq 9$.

LASSA consists of 9 individual telescopes which may be arranged in a variety of geometries. This array was built to provide isotopic identification of fragments ($Z < 10$) produced in low- and intermediate-energy heavy-ion reactions. In addition to good isotopic resolution, it was essential to provide a low threshold for particle identification as many of the fragments emitted in these reactions are low in energy.

Each LASSA telescope is composed of a stack of two silicon strip detectors followed by 4 CsI(Tl) crystals. The silicon which faces the target is 65 microns thick while the second silicon is 500 microns thick. Both silicons are ion-implanted passivated detectors, Si(IP). The 65 micron silicon wafer is segmented into 16 strips which are read out individually. The 500 micron wafer is segmented into 16 strips on its junction (front) side while the Ohmic surface (rear) is segmented into 16 strips in the orthogonal direction. Collection of holes and electrons in orthogonal directions provides two-dimensional position sensitivity from this detector alone. The additional position information from the 65 micron detector is used as a redundancy check. The pitch of the detector is nominally 3 mm with a 100 micron inter-strip gap. Behind the silicon detectors are 4 independent 6 cm CsI(Tl) crystals to stop penetrating particles. Scintillation caused by ionizing particles impinging on these scintillators is detected by 2 cm × 2 cm photodiodes (PD). The signals from the PD are amplified by pre-amplifiers mounted in the detector housing.

Each detector has 16 strips and an area of 5 cm by 5 cm. The detector set consists of a variety of ΔE and E detectors. The real ΔE detectors are 65 microns thick and are all one-sided for the readout. A set of 9 detectors 500 microns thick are double sided in readout. Finally, a set of 6 detectors are 1000 microns thick and are one sided. In the high-energy applications the 65 and 500 microns detectors are used backed with thick CsI(Tl) scintillators. For the Gammasphere applications only four of the 65 and 1000 microns telescopes are used. LASSA has been used in experiments at NSCL (Michigan State University), ATLAS (Argonne National Laboratory), and at the Cyclotron Institute (Texas A&M University).

3.2 HiRA

High Resolution Array [14].

3.2.1 General characteristics

– 20 telescopes Si(65 μm)-Si(1.5 mm)-CsI(Tl) read out by photodiode.
– For an amount of 1920 strips.

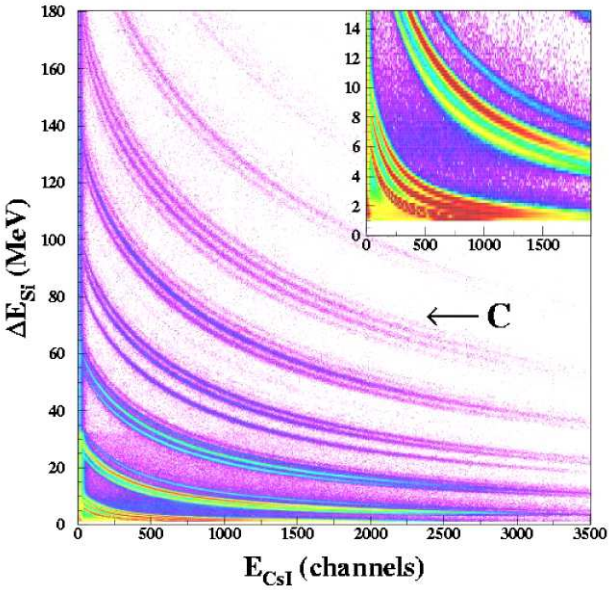

Fig. 4. An example of a ΔE-E matrix obtained with the LASSA-HIRA setup. The resolution for $Z = 1, 2$ is shown in the insert.

– Highly configurable for different experiments.

HiRA is an array of 20 telescopes with approximately three times the geometric efficiency of LASSA. This array is capable of addressing a wide range of physics goals including resonance spectroscopy, transfer reactions with radioactive ("exotic") beams, and reaction dynamics related to the equation of state. It was designed to develop a large solid-angle (high-efficiency) array of Si-Si-CsI(Tl) telescopes with high angular and energy resolution for radioactive-beam studies. The principal physics objectives of HiRA are elastic- and inelastic-scattering measurements with radioactive beams (important measurements in astrophysics), resonance spectroscopy, isospin dependence of the nuclear equation of state, and studies of nuclear-reaction dynamics. The design and construction of HiRA was built upon the experience in the design, construction, and performance of the LASSA array.

HiRA consists of 20 telescopes based upon a Si-Si-CsI(Tl) stack for identifying charged particles in Z and A by the ΔE-E technique. An example of a ΔE-E matrix for the Hira setup is presented in fig. 4. High isotopic resolution is obtained from H up to F. Each telescope is constructed from a 65 micron strip Si(IP) detector backed by a 1.5 mm silicon strip detector. The 65 micron detector is single-sided (32 strips on the junction (front) side only), while the 1.5 mm detector is segmented in 32 strips on the junction side with 32 orthogonal strips on the Ohmic (rear) surface. Thus the 1.5 mm will provide two-dimensional position information. The detectors have a 2 mm pitch with a 25 or 40 micron interstrip gap (junction and Ohmic surfaces, respectively).

4 Light ions

Bombarding light relativistic projectiles (π, p, C, ...) on much heavier nuclei allows to investigate the multifragment decay of a heavy target. This kind of study gives complementary information to that obtained from heavy-ion collisions and the comparison allows one to extract the influence of compression and rotation on the multifragment decay. Indeed for such collisions few compressional effects are expected as regards to central heavy-ion collisions. We therefore hope to explore a different portion of the phase diagram of hot nuclear matter.

4.1 ISIS

Indiana SIlicon Sphere.

4.1.1 General characteristics

- 162 individual telescopes covering 74% of 4π.
- Gas ionization chamber, 500 μm Si - 28 mm thick CsI(Tl) read out by photodiode.
- Each telescope measures Z, A, E and θ.
- Charge identification for Z with $0.6 \leq E/A \leq 96$ MeV.
- Isotopic separation for $Z \leq 4$ for $E/A \geq 8$ MeV.

The Indiana Silicon Sphere detector array is based on a spherical geometry, designed primarily for the study of light-ion–induced reactions. It consists of 162 triple telescopes, 90 in the forward hemisphere and 72 in the backward hemisphere, covering the angular ranges from 14° to 86.5° and 93.5° to 166°. The design consists of eight rings, each composed of 18 truncated-pyramid telescope housings. To increase granularity for the most forward angles, the ring nearest to 0° is segmented into two components. Each telescope is composed of: a gas-ionization chamber operated at 25–40 torr of CF4 or 12–20 torr of C3F8; a 500 μm ion-implanted passivated silicon detector, Si(IP), and a 28 mm thick CsI(Tl) crystal with light guide and photodiode readout. The telescope dynamic range permits measurement of $Z = 1$–20 fragments with discrete charge resolution over the dynamic range $0.6 \leq E/A \leq 96$ MeV. The Si(IP)/CsI(Tl) telescopes also provide particle identification (Z and A) for energetic H, He, Li and Be isotopes (E/A 8 MeV). The Si(IP) detectors constitute a critical component of the array in that they provide both excellent energy resolution and reliable energy calibration for the gas ionization chamber and CsI(Tl) elements.

4.2 FASA

4.2.1 General characteristics

- 55 thin scintillator crystals CsI(Tl).
- 5 time-of-flight telescopes.
- A large-area position-sensitive parallel-plate avalanche detector (PPAD).

The FASA setup [15], installed at the JINR synchrophasotron providing light ion beams with energies up to 3.65 GeV/nucleon, is a fragment multiplicity detector, consisting of 55 scintillation counters made of thin CsI(TI) films, five time-of-flight telescopes and a large-area position-sensitive parallel-plate avalanche chamber. The basic aim of the device is to determine with high precision the energy, mass, and velocity of the fragments detected in the time-of-flight telescopes (TOF) while for the other fragments global multiplicity information is obtained. Therefore, the TOF telescopes serve as a trigger. In addition, angular correlations and distributions and relative velocity correlations for coincident fragments can be measured. The FASA setup was also upgraded to FASA-2. Light-charged-particle (LCP) multiplicity detectors have been developed (64 plastic scintillator counters in the forward hemisphere). This gives the possibility to select the events according to impact parameter. A new detector system (25 ΔE(gas)-E(Si) telescopes) was made. It gives the better possibility for measuring IMF-IMF angular (and relative velocity) correlations, which are important for the time-scale study. This system is used also for triggering the FASA setup.

4.2.2 Main physics goals

In the FASA project the light relativistic projectiles from protons to carbon are used to investigate the multifragment decay of a heavy target. The study gives complementary information to that obtained from heavy-ion collisions, and the comparison allows one to extract the influence of compression and rotation on the multifragment decay.

5 Projectile decay fragmentation

Thanks to the forward focusing of the product emission in the laboratory frame (even better with increasing incident energy and reverse kinematic), many studies were performed on the decay of hot projectiles. Indeed in this case the complete angular coverage is not necessary as only the forward part is fired, reducing the number of detectors (and even their type as detection thresholds are not critical here) and associated electronics and thus the cost.

5.1 ALADIN

5.1.1 General characteristics

- Magnet.
- TP music.
- Time-of-flight wall.
- + coupling with LAND (Large Area Neutron Detector) [16].

5.1.2 Main ALADIN results

The ALADIN spectrometer, coupled with other detectors like the MINIBALL/wall [2], LAND [16] or Hodoscopes (for example, the Catania SIS Hodoscopes), was optimized for inverse-kinematics studies, namely projectile fragmentation at energies between 100 and 1000 A MeV: Au + C, Al, Cu, Pb at 600 A MeV, Au + Au at 100-250-400-1000 A MeV, Xe, Au, U + Be at 600-800-1000 A MeV [17]. Many aspect of multifragmenting projectiles were revealed, like the rise and fall in the fragment emission multiplicity with dissipation, collective expansion in central collisions, the universality behaviour of spectator fragmentation, the caloric curve of hot nuclei (T *vs.* E^* which shows the transition from a Fermi gas at low energy to a Boltzmann gas at higher energy), temperature measurements in exploding nuclei, break-up densities, ...

5.2 MULTICS

5.2.1 General characteristics

- 3 layers telescopes.
- Silicon 500 μm position sensitive.
- CsI(Tl) + photodiode.
- Angular coverage $3^\circ \leq \theta \leq 25^\circ$.
- Energy threshold $\simeq 1.5\,A$ MeV.
- Z identification up to the beam charge.

5.2.2 Main MULTICS results

Coupled with the MSU MINIBALL detector [2], experiments performed with the MULTICS-MINIBALL had a geometrical acceptance of 87% of 4π. Light charged particles and fragments with charge up to the beam charge were detected at θ_{lab} from 3° to 25° by the MULTICS array [8], with an energy threshold of about 1.5 A MeV, nearly independent of fragment charge. Light charged particles, $Z = 1$ and 2 isotopes and fragments with charge up to $Z \simeq 20$ were fully identified by 160 phoswich detector elements of the MSU MINIBALL, covering the angular range from 25° to 160°. The charge identification thresholds were about 2, 3, 4 A MeV for $Z = 3$, 10 and 18, respectively.

This setup device was mainly devoted to thermodynamical studies on the Au + Au system at 35 A MeV [18] and the search for signals of phase transition in nuclear matter: critical behaviour inside the coexistence region (critical exponent), caloric curve, exploration of the phase diagram of hot nuclear matter, negative heat capacity (associated to abnormal kinetic-energy fluctuations), scaling laws (Fisher's scaling), ...

5.3 FAUST

Forward Array Using Silicon Technology [19].

5.3.1 General characteristics

- 68 detectors: $1.6^\circ \leq \theta \leq 33.6^\circ$.
- 300 μm Si - 3 cm CsI(Tl) read out by photodiodes.
- Silicon are single area edge mounted.
- Isotopic resolution for $Z \leq 6$.
- Pulse-shape discrimination in CsI for light charged particles.

The FAUST detector was used for studying fragmentation of projectiles excited via peripheral interactions with heavy targets. This requires a forward array with relatively high granularity and good solid-angle coverage. Isotopic resolution of light fragments is also an additional dimension for these studies. FAUST is an array of 68 detector telescopes (Si-Csi(Tl) read out by photodiodes) arranged in five rings that are squares projected onto spherical surfaces. Ring 1 contains 8 telescopes and covers laboratory angles in the range $1.6^\circ \leq \theta \leq 4.5^\circ$. Ring 2 contains 12 telescopes and covers the range $4.6^\circ \leq \theta \leq 8.7^\circ$. Ring 3-5 each contain 16 detectors and cover angles in the ranges $8.8^\circ \leq \theta \leq 14.1^\circ$, $14.3^\circ \leq \theta \leq 22.4^\circ$ and $22.6^\circ \leq \theta \leq 33.6^\circ$. The mounting structure of each ring is hidden behind the active area of the ring in front of it. This combination provides a very good geometric coverage. The solid angular coverage from 2.3° to 33.6° is 89.7%. Isotopic resolution is obtained from $Z = 1$ up to charge $Z \simeq 6$ thanks to different identification techniques, namely ΔE-E for $Z \geq 2$ and pulse-shape discrimination applied to the signal coming from the CsI(Tl) for $Z \leq 3$.

5.3.2 Main FAUST results

The fragments resulting from the fragmentation have a source with a different N/Z than the initial beam. The N/Z present in the fragmenting system is on average not equal to the N/Z of the initial beam; there is a shift toward the valley of stability. Moreover there is a distribution in the N/Z of the fragmenting system, which appears to be isospin dependent. The overall dependence of the excitation energy on $(N/Z)_{QP}$ increases as the N/Z of the beam increases. Production of neutron-rich nuclides decreases with increasing excitation energy [20].

5.4 FIRST

Forward Indiana Ring Silicon Telescopes.

5.4.1 General characteristics

FIRST is a set of three annular Si-CsI(Tl) telescopes for the detection of the projectile-like fragment and forward-focused charged products. This array coupled to existing arrays such as LASSA is being built to better understand neck fragmentation and the projectile-fragmentation of radioactive ("exotic") beams. FIRST is intended to study the processes of neck and projectile fragmentation that

Table 1. Parameters of the three types of telescopes used in the FIRST array.

Designation	First element	Second element	Third element	No. of concentric rings	No. of pies
T1: 2.0°–7.0°	200–220 μm Si(IP)	1 mm Si(IP)	2 cm CsI(Tl)-PD	48	16
T2: 7.3°–14.5°	300 μm Si(IP)	2 cm CsI(Tl)/PD		16	16
T3: 15.0°–28.0°	300 μm Si(IP)	2 cm CsI(Tl)/PD		16	16

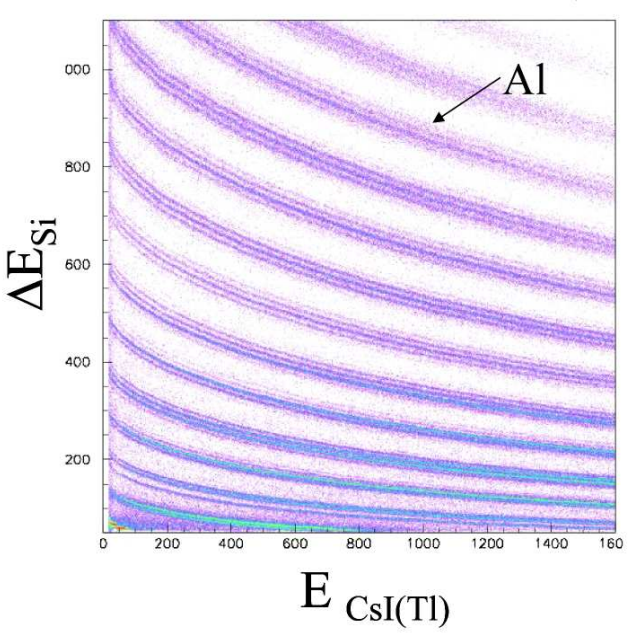

Fig. 5. A ΔE-E matrix for a FIRST telescope. Isotopic identification is performed up to Si, at least.

occurs for peripheral and mid-central collisions between two heavy ions.

FIRST consists of 3 telescopes based upon either a Si-Si-CsI(Tl) stack or just a Si-CsI(Tl) stack for identifying charged particles in Z and A by the ΔE-E technique. An example for the good isotopic resolution obtained with a First telescope over a wide range of elements is given in fig. 5. The most forward telescope is designated T1 and the more backward telescopes are T2 and T3, respectively. The parameters of the three telescopes are summarized in table 1.

5.5 ARGOS

5.5.1 General characteristics

The ARGOS multidetector [21] consists of 111 elements. Each element is a BaF2 crystal, 5 or 10 cm thick and of hexagonal shape, with a surface of 25 cm^2. An upgrade can be obtained just putting in front of the crystal a foil of plastic scintillator. In detecting a particle, the photo-multiplier signal is charge-integrated by two different gates, 20 and 300 ns wide, respectively. These fast and total (or slow) components together with the time-of-flight information allow charge identification for all detected particles, $Z < 30$, and mass identification for light charged particles and light ions. Due to the fast light response, timing characteristics of the detector are excellent, and time resolutions as low as 300 ps have recently been obtained, comprehensive of the beam burst width. Therefore, the neutron detection is also possible, with a measured efficiency between 5% and 20%, depending on the crystal thickness, neutron energy and electronic threshold. The elements can be assembled in different ways. In a typical geometry, the ARGOS "eyes" are distributed: 60 in a forward and 36 in a backward wall, both honeycomb shaped. As an example, for the first wall and for a distance of 2.35 m, all the particles in the angular range between 0.75° and 7° are detected. At the same time, for the backward wall at a distance of 50 cm, the angular range between 160° and 177° is covered.

6 High-resolution magnetic spectrometers

Full isotopic identification of the reaction residues over the whole mass range can be achieved by the use of high-resolution magnetic spectrometers. Experimental programs on nuclear-reaction dynamics have been performed at essentially three facilities, which will be listed in the following subsections. All three spectrometers have a common basic design, consisting of two stages with an intermediate dispersive and a final achromatic image plane. The projectile energies range from around 20 A MeV to 1 A GeV.

6.1 MARS recoil separator at Texas A&M University

6.1.1 General characteristics

The K500 superconducting cyclotron delivers beams with maximum energies from 20 to 50 A MeV, depending on the projectile mass. The MARS magnetic spectrometer [22] has an energy acceptance of ±9% and an angular acceptance of 9 msr. It can be positioned at angles between 0° and 30° with respect to the beam axis. Nuclide identification is performed by energy loss, residual energy, time of flight, and magnetic rigidity. ToF and position are measured by 2 PPACS, ΔE and E by a Si detector telescope. Important part of the ions with $Z > 12$ are not completely stripped, and thus the ionic-charge-state distribution has to be determined. The angular distribution up to 30° and the full momentum distribution of the reaction products can be determined by combining different measurements with different positions of the spectrometer and different magnetic fields.

6.1.2 Main results

The experiments with the MARS separator contribute to the institute's program in heavy-ion reaction dynamics and thermodynamics, investigating the properties and the decay modes of nuclear systems from low energy up to the limits of thermal and rotational stability, testing theories of many-body systems, chaotic-regime dynamics and the statistical mechanics of strongly interacting, finite quantum systems [23]. Systematic measurements in intermediate-energy heavy-ion collisions establish the degree of thermal, chemical and isospin equilibration, the mechanism of nuclear disassembly, the caloric curve and the mass and isospin dependence of limiting temperatures.

6.2 A1900 fragment separator at MSU, East Lansing

6.2.1 General characteristics

The coupled K500-K1200 cyclotrons deliver beams with maximum energies from 100 to 200 A MeV, depending on the projectile mass. The A1900 fragment separator [24] has a momentum acceptance of 5.5% and an angular acceptance of 8 msr. The heavier residues are fully transmitted. Nuclide identification is performed by Brho, ToF, and ΔE, which are measured by a scintillator, a PPAC, and a silicon detector telescope. Typically, reaction products with $Z < 30$ are fully stripped.

6.2.2 Main results

Systematic measurements of projectile fragments with full isotopic resolution for projectiles in the mass range around 50 to 60 have been performed, and their momentum distributions have been determined with the A1900 magnetic system [25]. The experiments are analyzed for testing and adapting dedicated model calculations of the nuclear-reaction process. A major aim is to optimize the production of exotic nuclei. Previously, a number of similar investigations had been performed with the A1200 system [26] at lower energies.

6.3 FRS magnetic spectrometer at GSI, Darmstadt

6.3.1 General characteristics

The heavy-ion synchrotron SIS18 delivers beams with maximum energies from 1 to 2 A GeV, depending on the projectile mass. The FRS magnetic spectrometer [27] has a momentum acceptance of ±2.5% and an angular acceptance of 15 mrad around the beam axis. This is adapted to full transmission of all heavier residues. For the lightest residues and fission fragments, the full momentum range can be obtained by combining different measurements, while the angular range is generally covered only up to 15 mrad. Nuclide identification is performed by Brho, ToF, and ΔE, which are measured by scintillation detectors and an ionization chamber. In figs. 6 and 7 we can see the good isotopic identification for all reaction products. Typically, they are fully stripped.

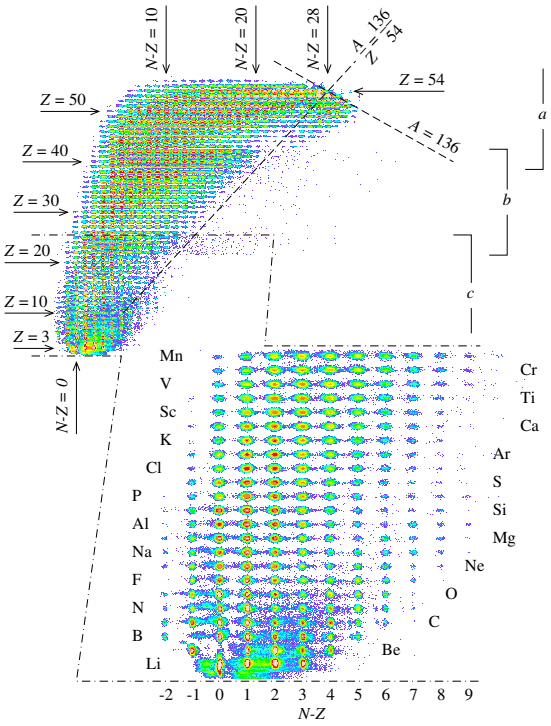

Fig. 6. Composition of all identified events measured with the FRS spectrometer with a ^{136}Xe beam at 1 A GeV on a hydrogen target. Three overlapping bands, a, b, c, correspond to the three groups of magnetic settings for the central isotopes ^{120}Ag, ^{69}Zn and ^{24}Al, respectively. The band c collecting light nuclides is enlarged in order to show the isotopic resolution (P. Napolitani, PhD Thesis, University Paris XI (2004)).

6.3.2 Main results

Dedicated experiments were performed on the identification of the projectile-like fragments and on their momentum distributions. The shift in the N/Z content during the evaporation cascade has been studied to determine the initial excitation energy introduced in the abrasion process [28] and to deduce the freeze-out temperature after thermal nuclear break-up [29]. The kinematical properties of projectile fragments produced in mid-peripheral collisions were introduced as a new access to study the nuclear equation of state, in particular to pin down the momentum dependence of the nuclear mean field [30]. This approach is complementary to the analysis of the flow pattern performed with 4π detectors up to now. A detailed analysis of the shape of the momentum distributions of the projectile fragments has been related to the decay characteristics of the excited spectators [31]. The charge-pickup channels provide information on the in-medium nucleon-nucleon cross-sections and the excitation of the Delta resonance [32].

6.3.3 Future projects

As the most promiment examples for next-generation magnetic systems, we concentrate on some new installa-

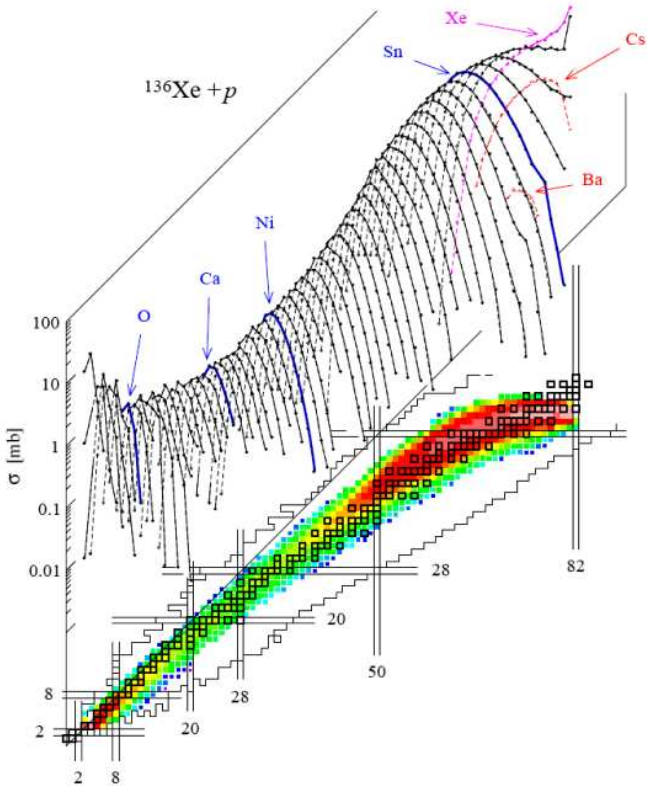

Fig. 7. Isotopic production cross-sections shown on a chart of nucleides for the reactions ^{136}Xe + p at 1 A GeV obtained with the FRS spectrometer (P. Napolitani, PhD Thesis, University Paris XI (2004)).

tions planned for the FAIR project [33]. The FAIR project currently represents a major step in the development of a new experimental installation, including more powerful magnetic spectrometers. The R3B project [34] aims for a large-acceptance dipole magnet with high resolution, which will combine isotopic resolution of all residues with simultaneous detection of light reaction products. Another important project is the Super-FRS [35], which follows the same ion-optical design as the present FRS with essentially larger acceptances in angle and momentum. Moreover, a pre-separator will facilitate the installation of additional detectors in the target area.

7 Neutron detection

In parallel to an always better charged-particle identification, it became rapidly evident that a lot of information was lost if neutron detection was missing. As neutron determination involves a different technique essentially incompatible with 4π detectors, since the coverage by silicon or scintillation detectors, plus their pre-amplifier, cooling system and so on, screen everything, it is very difficult to couple both charged particles and neutron detectors. Nonetheless, some experiments have tried to mix both techniques allowing compromise either on efficiency, granularity or particle identification and sometimes on intra-event correlation. In many cases part of the neutron information was obtained on their energy and/or their multiplicity. The combination ALADIN-LAND is an exception, since the magnet deflects the charged particles from the direction of the LAND detectors.

7.1 Rochester SUPERBALL

7.1.1 General characteristics

- Gd-doped liquid scintillator.
- Geometrical flexibility.
- Neutron multiplicity measured.
- Angular distribution given by 5 segments.
- Possibility of 4π charged particles in coincidence.

The University of Rochester SUPERBALL is a five-segment, 16000 liter gadolinium-loaded liquid scintillator 4π neutron calorimeter surrounding a vacuum scattering chamber. It delivers, through its 52 photomultiplier tubes, trains of electronic pulses in response to multi-neutron events. These trains contain information on neutron multiplicity (number of pulses in the train, excluding the prompt train head signal) and total kinetic energy of the injected neutrons (intensity of the prompt head signal). By its geometrical design, the SUPERBALL delivers additionally event-by-event angular information on the neutron yield. Its overall efficiency for neutrons from a 252-Cf fission-neutron source is 90% for typical threshold settings. The SUPERBALL measures the multiplicity of neutrons very efficiently. In addition, it measures the kinetic energies of neutrons and their emission directions. It surrounds the reaction chamber from all sides with a 1–1.5 m thick layer of scintillating liquid.

7.2 The National Superconducting Cyclotron Laboratory (NSCL) neutron walls

7.2.1 General characteristics

The neutron walls [36] are two large-area (2 m×2 m), high-efficiency, position-sensitive neutron detectors. Each wall consists of a stack of 25 glass cells filled with the scintillator liquid NE213, with which one can distinguish neutron from gamma-ray pulses by pulse-shape analysis. Each cell is two meters long and has phototubes at its ends. Light from an interaction in the liquid reaches the phototubes via total internal reflection. Each wall has its own carriage and can be positioned independently of the other. It is mainly devoted to extend our knowledge of the structure of exotic nuclei.

7.3 LAND

Large Area Neutron Detector [16].

7.3.1 General characteristics

- Overall dimension 2 m × 2 m × 1 m deep.
- 200 paddles of 200 cm × 10 cm area × 10 cm deep.
- Each paddle 11 sheets of Fe 2.5 mm/5 mm thick.
- Each paddle 10 sheets of 5 mm thick plastic scintillator.
- Alternating planes in perpendicular dimensions.
- Position resolution ±1 cm.

The LAND detector can be coupled to other devices installed at GSI-Germany in order to study different aspects of heavy-ion collisions.

Multifragmentation
The measurement of neutrons emerging from such a process allows to determine the excitation energy of the prefragments. For that purpose, LAND was installed in combination with a number of fragment detectors installed at the magnetic spectrometer ALADIN [17].

Collective flow of nuclear matter
The flow of neutral nuclear matter in (semi-)central heavy-ion collisions at high energy ($\lesssim 1\,A$ GeV) is studied employing LAND, operated in conjunction with the FOPI [11] charged-particle spectrometers. Directed flow ("squeeze-out") was observed in close resemblance to corresponding effects found for charged particles.

7.4 ORION

ORganic Interceptor Of Neutrons [37].

The ORION detector allows excitation-energy measurements of hot nuclei by observing the evaporated neutrons. It is constituted of 4200 liters of Gd-doped (0.3% of the weight) liquid scintillator (NE343). Light produced is collected by 22 photomultipliers. ORION is composed of separated modules of 1.60 m diameter covering the full solid angle and surrounding a large (1.30 m × 60 cm diameter) reaction chamber. For the amplification-transformation of the primary signals, photomultipliers are placed at the periphery of each module containing the liquid scintillator. The coincidence of at least 2 phototube-signals is required in order to reduce the influence of their intrinsic noise. The efficiency of the neutron detection is a function of the energy. The efficiency is quite high for neutrons of energy lower than 20 MeV which is the main region of interest for ORION measuring evaporation neutrons from sources of small velocity.

ORION is used for studies of:

- The properties of hot nuclei produced in heavy-ion–induced reactions or spallation reactions induced by light hadrons of several GeV.
- The influence of an existing halo of neutrons in a nucleus on the reaction mechanisms.
- The characteristics of spallation neutron sources.

7.5 DEMON: neutron wall

DÉtecteur MOdulaire de Neutrons [38].

DEMON is issued from a Belgian-French collaboration. It consists of a hundred individual large-size liquid-scintillator cells whose characteristics allow to accede to the angular and energy distributions of the emitted neutrons over a large energy range. DEMON is usually associated to master detectors. It has been conceived essentially to study the reaction mechanisms. But it can also be used in many other domains like in measurements of neutron halo, nuclear interferometry, or neutron cross-section for transmutation of nuclear waste. DEMON's modularity allows to adapt the geometry of the setup to particular needs. It has already been mounted in a cylindrical, a spherical and a wall configuration. DEMON consists of 100 individual large-size NE213 liquid-scintillator cells. Each cell is 20 cm long, has a diameter of 16 cm and contains 4.5 liters of liquid rich in hydrogen. A neutron coming into the scintillator interacts mainly with the protons which results in the ionization of the atoms of the scintillator. The subsequent de-excitation induces a light emission which has two components: a fast one and a slow one. The outcoming light is transformed into an electrical signal by a specially designed XP4512B photomultiplier tube. The shape analysis of this pulse allows the discrimination between incident neutrons and γ which have different slow components: a fast one and a slow one.

A proton rejection system (SYREP) is used to avoid proton contamination in the neutron spectra. DEMON operates in the atmosphere. Therefore, slow charged particles do not reach the scintillators. To avoid the contamination of the neutron spectra by very energetic protons which may reach the neutron detectors, DEMON disposes of 24 NE102 scintillators (3 mm thin) coupled to photomultipliers which can be mounted in front of the DEMON cells. These plastic scintillators are nearly 100% efficient to the protons and less than 0.5% to the neutrons. Thus, the protons can be rejected in the analysis of the data by an anti-coincidence between the two signals delivered by the two photomultipliers.

The n-γ discrimination is obtained by a pulse-shape analysis by comparison of the slow component of the charge to the total one. A very good discrimination is obtained down to 150 keV which corresponds to an energy of less than 1 MeV. DEMON has a high intrinsic efficiency over a large energy range: 50% for a neutron of 10 MeV and still 30% to 40% at 50 MeV. The energy of the neutrons is obtained by the measured time of flight with a resolution of 1.2 ns. The time of flight is corrected for the interaction distance inside the 20 cm deep cell. The geometrical acceptance of DEMON is of about 4–5% when the scintillators are at a distance of around 1.8 meters. The cross-talk of DEMON is very low and becomes negligible when the distance between two adjacent cells is of 16 cm.

8 Future detectors

With the availability of future radioactive beams (Spiral I-II, Eurisol, RIA, ...) it becomes clear that a complete charge and mass identification of all products coming from

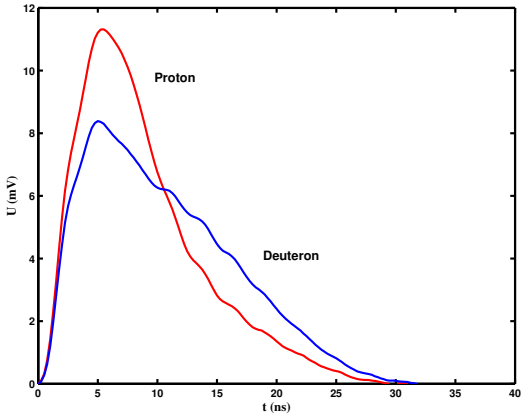

Fig. 8. Example of a mean experimental current signal sampling for two kind of particles, proton and deuteron, at the same incident energy of 5 MeV [39].

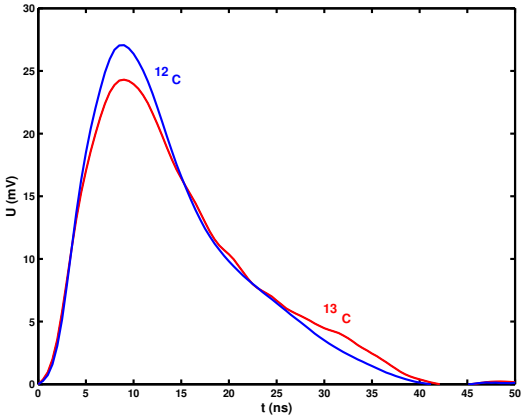

Fig. 9. Example of a mean experimental current signal sampling for two carbon isotopes, ^{12}C and ^{13}C, at the same incident energy of 80 MeV. Isotopic determination is well established with the second-moment values M_2 of digitized current pulse, see ref. [39] and fig. 10.

heavy-ions reactions will be necessary. This goal has only been reached with high-resolution spectrometers, which, however, are rather limited in their angular coverage and their momentum acceptance. Up to now, the maximum isotopic determination in multidetector systems is reached for $Z \simeq 10$ thanks to a ΔE-E method, usually Si-Si or Si-CsI. It is insufficient. New technological advances are necessary for the next generation of multidetector. This may be achieved either with the help of fast digital electronics coupled to appropriate detectors and a careful analysis of the pulse shape of the signals released by a particle crossing the detection material, see [39]. Figures 8 and 9 present different mean experimental current signal samplings for particles at the same energy, proton and deuteron at 5 MeV and two different carbon isotopes ^{12}C and ^{13}C at 80 MeV. If for light-particles discrimination is clearly observed, see fig. 8, for light fragments the use of the second-moment values M_2 is necessary to disentangle the two isotopes, see fig. 10.

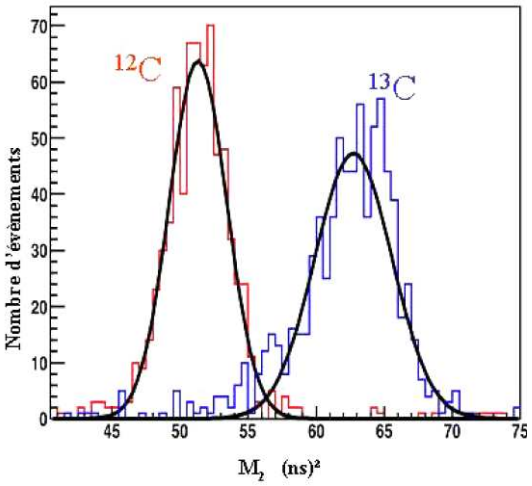

Fig. 10. Discrimination of carbon isotopes. Histograms correspond to the distributions of the second-moment values M_2 of the pulses and full lines to Gaussian fits, see [39].

Many groups all over the world are involved in research and developments on these topics. The final aim is to cover, by varying different techniques (ΔE-E, time of flight, pulse shape, ...), the widest isotopic range as possible.

Neutron detection (and light charged particles, Z = 1–2, of very high energy) are not forgotten in this context. Indeed when we are dealing with radioactive nuclei, neutron emission could be of very strong importance (chemical equilibration in time evolving processing, ...). Thus, more than ever their determination event by event is of first importance, including energy and multiplicity.

Morever we have learnt during the last decades that intra-event correlations are fundamental tools to extract precise information on the reaction process, either on time evolution, time emission, re-construction of hot fragments and thus calorimetry, volume determination, ... Therefore, still higher and higher granularity is requested, increasing angular resolution, reducing dead zones and multi-hits. Segmentation could be an issue, but for 4π detector it is a challenge.

What we have learnt so far with 4π multidetectors is the huge calibration time requested by such experiments. Months (even years) are usually necessary for complete and satisfactory results both on particle determination and their energy measurements. With a new generation of multidetectors the number of exit channels will explode. CHIMERA is at present constituted by 1192 telescopes Si-Csi(Tl). For the European project FAZIA (Four π A-Z Identification Array), 5000 to 6000 modules are envisaged, composed by a ΔE_1 (300 μm silicon), ΔE_2 (700 μm silicon) and a 4 cm crystal scintillator (CsI(Tl)). Moreover, pixel detectors are also still considered in the R&D project. It results, with such an amount of detectors, that calibration becomes one of the biggest challenges of such a program. Automatic procedures (neural networks, auto lines-recognition, ...) allowing to sample directly the particle characteristics (and not only their rough signals) are

envisaged. Those procedures are far from being reached but appear like a crucial goal, a key point of major importance.

9 Conclusion

Approaches based on multidetector systems have yielded many excellent and important results. Anyway the need for an always high-precision information is commonly recognized. Since the requirements to achieve large acceptance and high mass resolution are difficult in many aspects, for forward-focused heavy projectile-like fragments high-resolution magnetic spectrometers have been introduced as powerful tools. This approach provides full identification in A and Z of forward-focus reaction products as well as high-precision measurements of their longitudinal momentum with a resolution not reachable by multidetector systems alone. Nevertheless, complete event-by-event particle information is missing. The importance of isotopic identification of heavy residues being accepted, the combination of full-acceptance detectors for neutrons and light charged particles and intermediate mass fragment with high-resolution magnetic spectrometers for the heavier projectile-like fragments might be one way to combine the advantages of these two systems for certain reaction studies. For the others, a complete knowledge of the full intra-event correlations is necessary and only reachable with complete 4π multidetectors of a new generation.

References

1. DELF: R. Bougault *et al.*, Nucl. Instrum. Methods A **259**, 473 (1987); XYZt: G. Rudolf *et al.*, Nucl. Instrum. Methods A **307**, 325 (1991); MUR: G. Bizard *et al.*, Nucl. Instrum. Methods A **244**, 489 (1986); TONNEAU: A. Peghaire *et al.*, Nucl. Instrum. Methods A **295**, 365 (1990).
2. R.T. DeSouza *et al.*, Nucl. Instrum. Methods A **295**, 109 (1990).
3. D.R. Bowman *et al.*, Phys. Rev. Lett. **67**, 1527 (1991); Y.D. Kim *et al.*, Phys. Rev. Lett. **67**, 14 (1991).
4. J. Pouthas *et al.*, Nucl. Instrum. Methods A **357**, 418 (1995).
5. S. Aiello *et al.*, Nucl. Phys. A **583**, 561 (1995); S. Aiello *et al.*, Nucl. Instrum. Methods A **369**, 50 (1996); S. Aiello *et al.*, Nucl. Instrum. Methods A **400**, 469 (1997); M. Alderighi *et al.*, Nucl. Instrum. Methods A **489**, 257 (2002); N. Le Neindre *et al.*, Nucl. Instrum. Methods A **490**, 251 (2002).
6. A. Pagano *et al.*, Nucl. Phys. A **681**, 331c (2001); E. Geraci *et al.*, Nucl. Phys. A **732**, 173 (2004); A. Pagano *et al.*, Nucl. Phys. A **734**, 504 (2004); E. De Filippo *et al.*, Phys. Rev. C **71**, 044602 (2005); E. De Filippo *et al.*, Phys. Rev. C **71**, 064604 (2005).
7. F. Gramegna *et al.*, Nucl. Instrum. Methods A **389**, 474 (1997); U. Abbondanno *et al.*, Nucl. Instrum. Methods A **488**, 604 (2002).
8. I. Iori *et al.*, Nucl. Instrum. Methods A **325**, 458 (1993); M. Bruno *et al.*, Nucl. Instrum. Methods A **311**, 189 (1992); N. Colonna *et al.*, Nucl. Instrum. Methods A **321**, 529 (1992); P.F. Mastinu *et al.*, Nucl. Instrum. Methods A **338**, 419 (1994).
9. M. Bini *et al.*, Nucl. Instrum. Methods A **515**, 497 (2003).
10. See `http://cyclotron.tamu.edu/nimrod/`.
11. A. Gobbi *et al.*, Nucl. Instrum. Methods A **324**, 156 (1993).
12. W. Reisdorf *et al.*, Nucl. Phys. A **612**, 493 (1997); F. Rami *et al.*, Phys. Rev. Lett. **84**, 1120 (2000); P. Crochet *et al.*, Phys. Lett. B **486**, 6 (2000); W. Reisdorf *et al.*, Phys. Rev. Lett. **92**, 232301 (2004).
13. E. Migneco *et al.*, Nucl. Instrum. Methods A **314**, 31 (1992); MACISTE, IEEE Trans. Nucl. Sci. **43**, 1737 (1996).
14. A. Wagner *et al.*, Nucl. Instrum. Methods A **456**, 290 (2000); B. Gavin *et al.*, Nucl. Instrum. Methods A **473**, 301 (2001).
15. S.P. Avdeyev *et al.*, Nucl. Instrum. Methods A **332**, 149 (1993).
16. Th. Blaich *et al.*, Nucl. Instrum. Methods A **314**, 136 (1992).
17. C.A. Ogilvie *et al.*, Phys. Rev. Lett. **67**, 1214 (1991); W.C. Hsi *et al.*, Phys. Rev. Lett. **73**, 3367 (1994); A. Schüttauf *et al.*, Nucl. Phys. A **607**, 457 (1996); J. Pochodzalla *et al.*, Phys. Rev. Lett. **75**, 1040 (1995); V. Serfling *et al.*, Phys. Rev. Lett. **80**, 3928 (1998); S. Fritz *et al.*, Phys. Lett. B **461**, 315 (1999); T. Odeh *et al.*, Phys. Rev. Lett. **84**, 4557 (2000).
18. M. D'Agostino *et al.*, Nucl. Phys. A **650**, 329 (1999); M. D'Agostino *et al.*, Phys. Lett. B **473**, 219 (2000); M. D'Agostino *et al.*, Nucl. Phys. A **699**, 795 (2002); M. D'Agostino *et al.*, Nucl. Phys. A **724**, 455 (2003); M. D'Agostino *et al.*, Nucl. Phys. A **734**, 512 (2004).
19. F. Gimeno-Nogues *et al.*, Nucl. Instrum. Methods A **399**, 94 (1997); R. Laforest *et al.*, Nucl. Instrum. Methods A **404**, 470 (1998).
20. D.J. Rowland *et al.*, Phys. Rev. C **67**, 064602 (2003).
21. G. Lanzano *et al.*, Nucl. Instrum. Methods A **323**, 694 (1992); G. Lanzano *et al.*, Nucl. Phys. A **683**, 566 (2001).
22. R.E. Tribble *et al.*, Nucl. Instrum. Methods A **285**, 441 (1989).
23. G.A. Souliotis *et al.*, Phys. Rev. C **68**, 024605 (2003); G.A. Souliotis *et al.*, Phys. Lett. B **588**, 35 (2004).
24. D.J. Morrissey, NSCL Staff, Nucl. Instrum. Methods B **26**, 316 (1997); D.J. Morrissey *et al.*, Nucl. Instrum. Methods B **204**, 90 (2003).
25. M. Mocko *et al.*, Nucl. Phys. A **734**, 532 (2004); A. Stolzet *et al.*, Phys. Lett. B **627**, 32 (2005).
26. R. Pfaff *et al.*, Phys. Rev. C **51**, 1348 (1995); K.A. Hanold *et al.*, Phys. Rev. C **52**, 1462 (1995); R. Pfaff *et al.*, Phys. Rev. C **53**, 1753 (1996); G.A. Souliotis *et al.*, Phys. Rev. C **57**, 3129 (1998); G.A. Souliotis *et al.*, Nucl. Phys. A **705**, 279 (2002).
27. H. Geissel *et al.*, Nucl. Instrum. Methods B **70**, 286 (1992).
28. K.-H. Schmidt *et al.*, Phys. Lett. B **300**, 313 (1993).
29. K.-H. Schmidt *et al.*, Nucl. Phys. A **710**, 157 (2002).
30. M.V. Ricciardi *et al.*, Phys. Rev. Lett. **90**, 212302 (2003).
31. P. Napolitani *et al.*, Phys. Rev. C **70**, 054607 (2004).
32. A. Kelic *et al.*, Phys. Rev. C **70**, 064608 (2004).
33. `http://www.gsi.de/fair/index.html`.
34. `http://www-land.gsi.de/r3b/index.html`.
35. H. Geissel *et al.*, Nucl. Instrum. Methods B **204**, 71 (2003).
36. P.D. Zecher *et al.*, Nucl. Instrum. Methods A **401**, 329 (1997).

37. Y. Périer *et al.*, Nucl. Instrum. Methods A **413**, 321 (1998).
38. G. Bizard *et al.*, Nucl. Phys. News **1**, No. 5, 15 (1991); M. Moszynski *et al.*, Nucl. Instrum. Methods A **307**, 97 (1991); M. Moszynski *et al.*, Nucl. Instrum. Methods A **317**, 262 (1992); M. Moszynski *et al.*, Nucl. Instrum. Methods A **343**, 563 (1994); M. Moszynski *et al.*, Nucl. Instrum. Methods A **350**, 226 (1994); S. Mouatassim *et al.*, Nucl. Instrum. Methods A **359**, 530 (1995); I. Tilquin *et al.*, Nucl. Instrum. Methods A **365**, 446 (1995).
39. H. Hamrita *et al.*, Nucl. Instrum Methods A **531**, 607 (2004) and PhD Thesis, University Paris VI (2005).